Chapter 1

Introduction

1.1 Solution methods

The governing equations for the motion of a fluid are nonlinear PDEs. Due to the difficulty in solving these transport equations, which do not have closed-form solutions except in very special cases, experiments have been widely used in the analysis and design of devices that require knowledge of the flow-field, such as aircraft, engines, ducts or heat exchangers. The *experimental approach* to the solution of fluid problems requires building an experimental apparatus and measuring the desired quantities. It is based on the assumption that full dynamic similarity can be achieved (to ensure that the forces acting on the model are the same as those acting on the prototype), and that all the desired quantities can be measured with satisfactory accuracy. Although experiments often realize the closest possible approximation of a configuration of interest, it is frequently hard to measure some quantities (pressure for instance) with sufficient accuracy; furthermore, multi-point measurements are difficult. Finally, experiments are very expensive and time-consuming, and it is generally unfeasible to perform optimization studies examining a large parameter space experimentally.

Although the governing PDEs are not amenable to analytical solution, they can sometimes be simplified to such an extent that *semi-analytical* solutions can be found, with the aid of experimental data (in the form of correlations, usually) and often of computers to integrate numerically ODEs or to evaluate integrals, or invert large systems of algebraic equations. This theoretical approach is restricted to the cases where enough simplifications can be made on the governing equations and boundary conditions.

Alternatively, one can discretize the governing equations (*i.e.*, approximate the derivatives by differences evaluated over discrete points), and transform directly the nonlinear PDEs into sets of algebraic (linear or nonlinear equations) that can be solved numerically. The numerical solution of fluid dynamical problems (or Computational Fluid Dynamics - CFD) requires the availability of advanced computers. Its main advantage over the analytical approach is that fewer assumptions are required, and more complex problems can be handled. Furthermore it is faster and cheaper (usually) than experiments, and provides more detailed information. Unlike the theory, however, CFD requires interpretation before trends can be derived, and very careful control of the numerical errors must be performed to avoid unphysical solutions.

Numerical techniques can be applied to governing equations corresponding to any level of complexity. In decreasing order, the equations that can be solved are:

1. Viscous flows:
   (a) Direct Simulation of the Navier-Stokes equations (DNS).
   (b) Large-eddy simulation of the Navier-Stokes equations (LES).
   (c) Solution of the Reynolds-Averaged Navier-Stokes equations (RANS).
   (d) Solution of the Thin Shear Layer (TSL) equations.
   (e) Solution of the Parabolized Navier-Stokes (PNS) equations.
   (f) Solution of the boundary-layer equations.
2. Inviscid flows:

(a) Solution of the Euler equations.
(b) Solution of the Full Potential Equations (FPE).
(c) Solution of the Linearized Transonic Small-Disturbance Equations (TSD).
(d) Solution of the Prandtl-Glauert equations for compressible flows.
(e) Solution of Poisson's or Laplace's equations for incompressible potential flows.

Descending this list, the number of simplifying assumptions regarding the nature of the flow increases. Correspondingly, the cost of the calculations decreases (for a given geometry). Depending on the application, a compromise must be reached to obtain the highest degree of accuracy possible within some computational cost constraints. Applications to complex geometries typically require lower-level approximations, whereas very detailed analyses can be performed, using DNS or LES, on simpler configurations.

1.2 Governing equations

1.2.1 Conservation of mass (continuity equation)

$$\frac{\partial \rho}{\partial t} + \frac{\partial}{\partial x_j}(\rho u_j) = 0 \tag{1.1}$$

For incompressible flow:

$$\frac{\partial u_j}{\partial x_j} = 0 \tag{1.2}$$

1.2.2 Conservation of momentum for a Newtonian fluid (Navier-Stokes Equations)

$$\frac{\partial}{\partial t}\rho u_i + \frac{\partial}{\partial x_j}\left[\rho u_i u_j + \delta_{ij} p - \tau_{ij}\right] = \rho f_i \tag{1.3}$$

$$\tau_{ij} = \mu \left[\left(\frac{\partial u_i}{\partial x_j} + \frac{\partial u_j}{\partial x_i}\right) - \frac{2}{3}\delta_{ij}\frac{\partial u_k}{\partial x_k}\right] \tag{1.4}$$

For incompressible flow:

$$\frac{\partial u_i}{\partial t} + \frac{\partial}{\partial x_j}\left[u_i u_j + \frac{\delta_{ij} p}{\rho} - \frac{\tau_{ij}}{\rho}\right] = f_i \tag{1.5}$$

$$\tau_{ij} = \mu \left(\frac{\partial u_i}{\partial x_j} + \frac{\partial u_j}{\partial x_i}\right) \tag{1.6}$$

1.2.3 Conservation of total energy

$$E_t = \rho\left(e + \frac{V^2}{2}\right) = \rho\left(c_v T + \frac{1}{2}u_i u_i\right) \tag{1.7}$$

$$\frac{\partial E_t}{\partial t} + \frac{\partial}{\partial x_j}\left[(E_t + p)\, u_j - k\frac{\partial T}{\partial x_j} - \tau_{kj} u_k\right] = \frac{\partial Q}{\partial t} + \rho f_j u_j, \tag{1.8}$$

where $E_t = C_v T + \rho u_i u_i/2$. For incompressible flows, the energy equation is decoupled from the momentum equations and takes the form:

$$\begin{aligned}\frac{\partial H}{\partial t} &+ \frac{\partial}{\partial x_j}\left[H u_j - k\frac{\partial T}{\partial x_j} - p u_j\right] = \Phi \\ &+ \frac{\partial p}{\partial t} + \frac{\partial Q}{\partial t} + \rho f_j u_j\end{aligned} \tag{1.9}$$

$$H = \rho e + p = \rho c_p T \tag{1.10}$$

$$\Phi = \tau_{ij}\frac{\partial u_i}{\partial x_j} \tag{1.11}$$

1.2.4 Filtered equations of motion

In turbulent flows a very wide range of scales (eddies) is present; the largest eddies depend on the boundary conditions, and are difficult to model in a universal way; the smallest scales, on the other hand, are more homogeneous, isotropic and universal and can be more easily parameterized. To separate the large from the small eddies one can introduce a filtering operation: a filtered (or resolved, or large-scale) variable, denoted by an overbar, is defined as

$$\overline{f}(\mathbf{x}) = \int_D f(\mathbf{x}')G(\mathbf{x},\mathbf{x}')d\mathbf{x}', \tag{1.12}$$

where D is the entire domain and G is the *filter* function. The filter function determines the size and structure of the small scales. It is easy to show that, if G is a function of $x - x'$ only, differentiation and the filtering operation commute.

If the filtering operation (1.12) is applied to the governing equations, one obtains the filtered equations of motion, which are solved in large-eddy simulations. For an incompressible flow of a Newtonian fluid, they take the following form:

$$\frac{\partial \overline{u}_i}{\partial x_i} = 0. \tag{1.13}$$

$$\frac{\partial \overline{u}_i}{\partial t} + \frac{\partial}{\partial x_j}(\overline{u}_i\overline{u}_j) = -\frac{1}{\rho}\frac{\partial \overline{p}}{\partial x_i} - \frac{\partial \tau_{ij}}{\partial x_j} + \nu\frac{\partial^2 \overline{u}_i}{\partial x_j \partial x_j}. \tag{1.14}$$

The filtered Navier-Stokes equations, written above, govern the evolution of the large, energy-carrying, scales of motion. The effect of the small scales appears through a subgrid-scale (SGS) stress term,

$$\tau_{ij} = \overline{u_i u_j} - \overline{u}_i\overline{u}_j, \tag{1.15}$$

that must be modeled. The approach in which the filtered equations (1.13–1.14) are solved and the SGS stresses τ_{ij} are modeled is called *large-eddy simulation* (LES).

1.2.5 Reynolds-averaged Navier-Stokes equations

Several types of averaging procedures are used in turbulent flows to separate the effects of the fluctuating turbulent motions from the average (mean) flow. Among them are the *time average*, the *ensemble average*, and the *spatial average*. The *time average* of a stationary random variable $U(t)$ (*i.e.*, one whose statistics are time-invariant) is defined as

$$\overline{U} = \frac{1}{T}\int_t^{t+T} U(t')dt', \tag{1.16}$$

where T is a time-scale, much longer than the time-scale of the turbulent fluctuations. For non-stationary processes, the *ensemble average* is preferred, which is defined as

$$\overline{U} = \frac{1}{N}\sum_{n=1}^{N} U(t_n), \tag{1.17}$$

where the sum is taken over N different realizations, but at corresponding times, t_n, of the non-stationary process.

Both time- and ensemble-averages are examples of *Reynolds averages*. Let

$$A = \overline{A} + a, \tag{1.18}$$

where the lower case symbol indicates a fluctuation about the average (or mean) value. The following rules, whose simple proof is left to the reader, apply to Reynolds-averaged quantities:

1. $\overline{a} = 0$ (from the definition 1.16).

2. $\overline{\overline{A}} = \overline{A}$ (also from 1.16 and property 1).

3. $\overline{\overline{A}\,\overline{B}} = \overline{\overline{A}}\,\overline{\overline{B}} = \overline{A}\,\overline{B}$ (*i.e.*, the average of the product of two mean values is the product of the mean values).

4. $\overline{\overline{A}b} = \overline{\overline{A}}\,\overline{b} = 0$, (*i.e.*, the average of the product of a mean value and a fluctuation about a mean value is zero because $\overline{b} = 0$.)

5. $\overline{AB} = \overline{(\overline{A} + a)(\overline{B} + b)} = \overline{A}\,\overline{B} + \overline{ab}$.

6. $\overline{\partial A/\partial x} = \partial \overline{A}/\partial x$, (*i.e.*, Reynolds-averaging commutes with differentiation.)

7. $\overline{A + B} = \overline{A} + \overline{B}$, (*i.e.*, Reynolds-averaging commutes with addition.)

Mass conservation

Consider conservation of mass for an incompressible flow in a rectangular coordinate system:

$$\frac{\partial U_i}{\partial x_i} = 0, \tag{1.19}$$

where U_i is the instantaneous velocity in one of the coordinate directions, and x_i is a coordinate direction. If we decompose the velocity U_i into mean and fluctuating parts

$$U_i = \overline{U}_i + u_i, \tag{1.20}$$

and substitute the Reynolds' decomposition (1.20) into (1.19), and then take a time- or ensemble-average of the resulting equations, we obtain

$$\frac{\partial}{\partial x_i}(\overline{\overline{U}_i + u_i}) = 0. \tag{1.21}$$

Applying Reynolds' rules of averaging, in particular, rules 4 and 6, gives

$$\frac{\partial \overline{U}_i}{\partial x_i} = 0, \tag{1.22}$$

$$\frac{\partial u_i}{\partial x_i} = 0, \tag{1.23}$$

which indicate that both the mean and the fluctuating velocities are divergence-free.

Momentum conservation

Consider now the Navier-Stokes equation for an incompressible flow:

$$\rho\frac{\partial U_i}{\partial t} + \rho\frac{\partial}{\partial x_k}(U_k U_i) = -\frac{\partial P}{\partial x_i} + \mu\nabla^2 U_i, \tag{1.24}$$

where P is the instantaneous fluid pressure, and ρ and μ are the fluid density and viscosity. Substituting again the Reynolds' decomposition into (1.24), and averaging each term in the equation following Reynolds' rules, gives

$$\rho\left[\frac{\partial \overline{U}_i}{\partial t} + \frac{\partial}{\partial x_k}\left(\overline{U}_k\overline{U}_i\right)\right] = -\frac{\partial \overline{P}}{\partial x_i} + \frac{\partial}{\partial x_k}\left(\mu\frac{\partial \overline{U}_i}{\partial x_k} - \rho\overline{u_i' u_k'}\right); \tag{1.25}$$

which is the transport equation for the average momentum in the x_i direction. The set formed by (1.22) and (1.25) is known as *Reynolds' equations*, and also as the *Reynolds-averaged Navier-Stokes (RANS) equations*.

The Reynolds equations have an additional dependent variable, the *Reynolds stress tensor* $-\rho\overline{u_i' u_j'}$, which is a tensorial correlation between velocity fluctuations. It can also be thought of as a turbulent momentum flux, since it acts on the flow as a set of additional (apparent) stresses, just as the diffusive momentum flux gives rise to the viscous stresses, $\mu(\partial\overline{U}_i/\partial x_j)$. If we consider, for example, the mean rate at which the x_1-component of momentum is transported into a face $dx_1 dx_3$ of a differential control volume, *i.e.*, the mean of the product of the mass flow-rate in the x_2-direction, $\rho(\overline{U}_2 + u_2)dx_1dx_3$ by the velocity in the x_1-direction, $(\overline{U}_1 + u_1)$, we obtain

$$\overline{(\overline{U}_1 + u_1)\,\rho(\overline{U}_2 + u_2)}\,dx_1dx_3 = \rho(\overline{U}_1\overline{U}_2 + \overline{u_1u_2})dx_1dx_3. \tag{1.26}$$

The transport of mean momentum into the control volume is strongly affected by the fluctuations (the $\overline{u_1u_2}$ component of the Reynolds stress tensor, here viewed as momentum flux) although the mean momentum per unit volume of each fluctuating component individually is zero, *i.e.*, $\rho\overline{u_i} = 0$.

The Reynolds stress tensor is symmetric. Its diagonal terms are the *normal Reynolds stresses* $\rho\overline{u_\alpha u_\alpha}$ (no summation is applied over repeated Greek indices), while the other three independent terms $\rho\overline{u'_iu'_j}$ $(i \neq j)$ are the *Reynolds shear stresses*. In turbulent pipe flow, with turbulent fluctuations that are $\pm 10\%$ of the centerline velocity, the Reynolds stresses $-\rho\overline{u'_iu'_j}$ are two orders of magnitude larger than the mean viscous stresses $2\mu\overline{S}_{ij}$, which illustrates their important role in determining the mean motion.

1.2.6 Euler equations

$$\frac{\partial\rho}{\partial t} + \frac{\partial}{\partial x_j}(\rho u_j) = 0 \tag{1.27}$$

$$\frac{\partial}{\partial t}\rho u_i + \frac{\partial}{\partial x_j}[\rho u_iu_j + \delta_{ij}p] = \rho f_i \tag{1.28}$$

$$\frac{\partial E_t}{\partial t} + \frac{\partial}{\partial x_j}[(E_t + p)\,u_j] = \rho\mathbf{f}\cdot\mathbf{V} \tag{1.29}$$

1.2.7 Full potential equations

The full potential equations are valid in inviscid, irrotational, steady, isentropic flow. They take the form

$$u_j = \frac{\partial\phi}{\partial x_j} \tag{1.30}$$

$$\left(1 - \frac{\phi_x}{a^2}\right)\phi_{xx} + \left(1 - \frac{\phi_y}{a^2}\right)\phi_{yy} - \frac{2}{a^2}\phi_x\phi_y\phi_{xy} = 0 \tag{1.31}$$

$$a = \sqrt{\gamma RT} \tag{1.32}$$

1.2.8 Transonic small-disturbance equation

The transonic small-disturbance equation are valid for an inviscid, irrotational, steady, isentropic, and for a slender body. They are of the form

$$\phi = \Phi + \phi' \tag{1.33}$$

$$\left[\left(1 - M_\infty^2\right) - (\gamma + 1)\,M_\infty^2\right]\phi'_{xx} + \phi'_{yy} = 0 \tag{1.34}$$

$$M_\infty = \frac{V_\infty}{a} = \frac{1}{a}\frac{\partial\Phi}{\partial x} \tag{1.35}$$

1.2.9 Prandtl-Glauert equation

The Prandtl-Glauert equation are valid in inviscid, irrotational, steady, isentropic, for a slender body and $M_\infty \neq 1$. They take the form

$$\left(1 - M_\infty^2\right)\phi'_{xx} + \phi'_{yy} = 0 \tag{1.36}$$

1.2.10 Boundary conditions and constitutive equations

To close the problem, constitutive relations (equation of state, Sutherland's law of viscosity etc.) and sometimes models (for the Reynolds or SGS stresses) are required, as well as boundary conditions.

In viscous flows, the no-slip condition is applied at solid boundaries; in inviscid flows, the boundary is required to be impermeable. At solid walls, a Neumann condition for the pressure is usually applied (which is required in numerical solutions, not by the mathematical formulations):

$$\frac{\partial p}{\partial n} = -\rho \frac{u_i u_i}{2} + \frac{\partial \tau_{nn}}{\partial n} \tag{1.37}$$

where the second term is only present in viscous flows and n is the coordinate normal to the surface.

At free surfaces, characteristic conditions are usually applied. The number of quantities that must be specified depends on whether the flow is subsonic or supersonic.

1.3 Applications of CFD

CFD has been widely applied both by the research community, and by industry. By and large, research applications are driven by the need of understanding the physical phenomena that govern some particular flow, often that is difficult to realize experimentally. They give very detailed information with high order of accuracy, using special-purpose numerical codes in which the numerics are carefully (hopefully) controlled, and minimal amounts of modeling are performed.

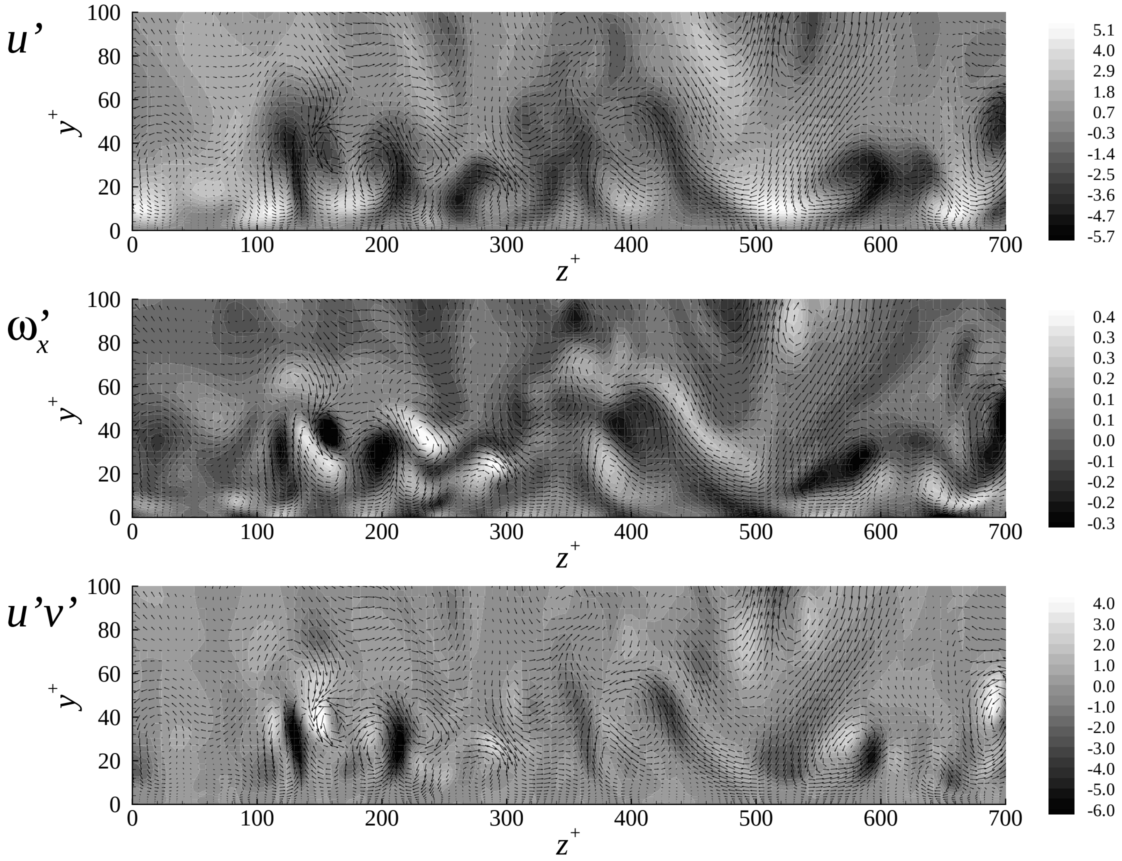

Figure 1.1: Velocity, vorticity, Reynolds stress contours and secondary $(v - w)$ velocity vectors in a cross-plane. The flow is in the direction normal to the $yz-$plane. Turbulent plane channel flow, $Re_\tau = 180$.

Direct numerical simulations, for instance, supply the time-dependent velocity field at multiple locations in the flow, yielding a wealth of information from which single- and multi-point statistics can be calculated,

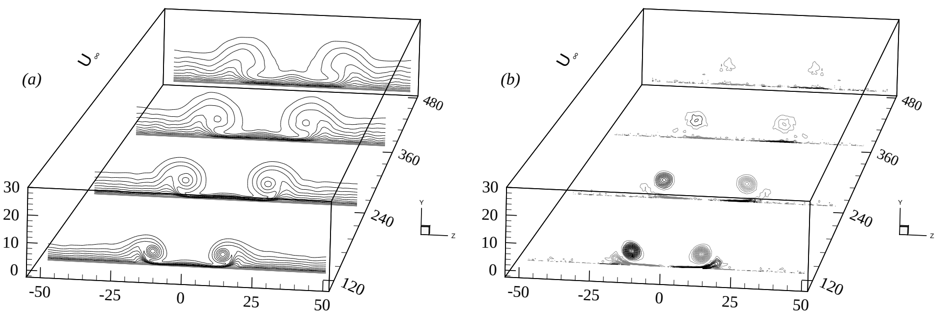

Figure 1.2: Vortex/boundary layer interaction. (a) Contours of the mean streamwise velocity U. (b) Contours of the mean streamwise vorticity Ω_x.

even for quantities (such as the pressure or the vorticity) that are difficult to measure experimentally. Figure 1.1, for instance, highlights the relationship between the sweeps (regions of high-speed fluid moving towards the wall), the quasi-streamwise vortices, and the regions of large Reynolds stress $u'v'$. Around $z^+ = 150$, for example, several quasi-streamwise vortical structures can be observed; very close to these structures, regions of high Reynolds shear stress are located.

Large-eddy simulations can also be used to study in detail the physics of simple flows. Liu *et al.* [6] computed the flow in a turbulent boundary layer on which a pair of strong counter-rotating vortices was superimposed, using a localized dynamic model. The vortices generate the extra strain components $\partial V/\partial y$, $\partial V/\partial z$, $\partial W/\partial y$ and $\partial W/\partial z$. The mean streamwise vorticity development is shown in Fig. 1.2. Near the wall, under the principal vortices, secondary vorticity of the opposite sign is generated, which decay more slowly than the primary one, and lifted by the primary vortices.

The Reynolds-averaged Navier-Stokes equations were solved by Khorramy *et al.* [4] to study the flow around the edge of a flap. The configuration is too complex to allow more basic methods. Nonetheless, the calculations capture very well the vortex generated at the flap edge, as well as its motion. These finding are used to determine airframe sound emission during take-off and landing.

Industrial applications of CFD are driven by the need to bypass wind-tunnel testing, which is not suited to be integrated in the design process. CFD codes need to be robust (*i.e.*, be applicable to a wide variety of flow configurations), reliable, quick, and predict at least the trends accurately. Fig. 1.4 shows two applications of CFD to external flows.

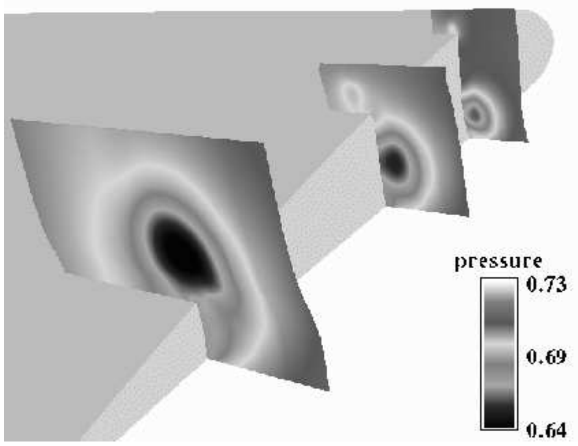

Figure 1.3: Pressure field at the edge of a flap (from Khorramy *et al.* [4]).

1.4 Building a CFD solution

In this section, some basic concept for CFD applications will be outlined by presenting examples of solution methods for CFD problems, in a step-by-step fashion, highlighting the possible sources of errors involved in each step.

1.4.1 Choose the model

First, one must choose the appropriate set of governing equations (Euler, Navier-Stokes, Reynolds equations). This step requires that simplifications be made and that the appropriate closures (for the Reynolds stresses, for instance) be chosen ⇒ **Modeling errors**.

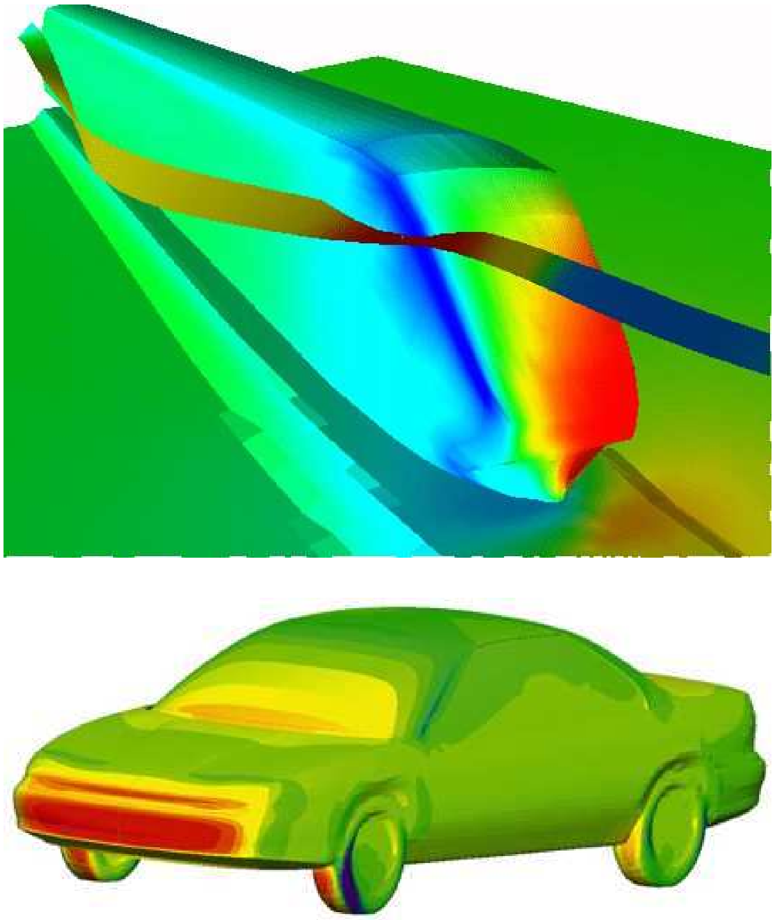

Figure 1.4: Examples of industrial applications of CFD. Top: pressure field around a train in a crossflow (calculations by AEA); : pressure field around a dodge Intrepid (calculations by CFD Research Corporation)

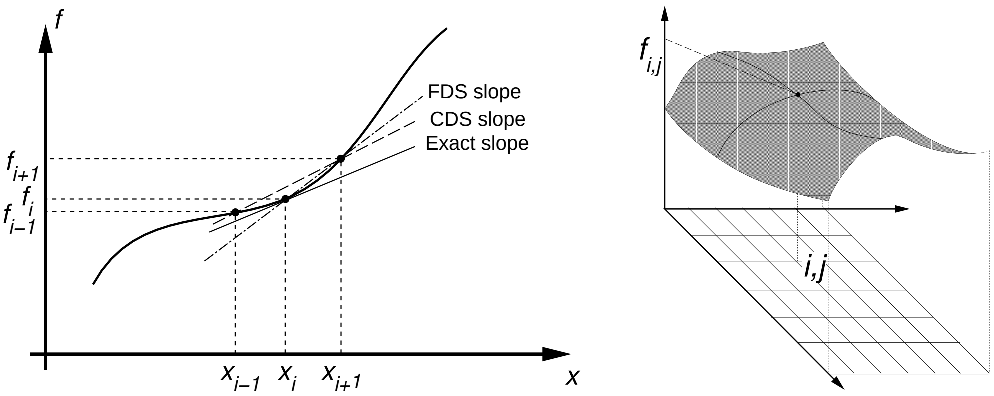

Figure 1.5: Discrete approximation of a function and its derivatives in one (left) and two (right) spatial dimensions.

1.4.2 Choose the discretization method

Several possibilities are available: finite differences, volumes or elements, or spectral methods. Some error is always introduced when representing a continuous function on a discrete mesh ⇒ **Discretization errors**.

Finite differences

We introduce the discretization (*grid*) and evaluate the derivatives at discrete points (*nodes*), using the Taylor series expansions to obtain the derivatives using other nodal values; any order of accuracy can be achieved; for example (Fig. 1.5) the following approximations can be used:

$$\begin{aligned}\frac{df_i}{dx} &= \lim_{\Delta x \to 0} \frac{f(x_i+\Delta x)-f(x_i)}{\Delta x} \simeq \frac{f(x_i+\Delta x)-f(x_i)}{\Delta x} \\ &\simeq \frac{f(x_{i+1})-f(x_i)}{\Delta x} \qquad \text{(FDS)} \qquad (1.38)\\ &\simeq \frac{f(x_{i+1})-f(x_{i-1})}{2\Delta x} \qquad \text{(CDS)} \qquad (1.39)\\ &\simeq \frac{f(x_i)-f(x_{i-1})}{\Delta x} \qquad \text{(CDS)} \qquad (1.40)\end{aligned}$$

which are called, respectively, *forward*, *central* and *backward* approximations. Similarly in two or more dimensions:

$$\frac{\partial f_{i,j}}{\partial x} \simeq \frac{f_{i+1,j}-f_{i,j}}{\Delta x}; \qquad \frac{\partial f_{i,j}}{\partial y} \simeq \frac{f_{i,j+1}-f_{i,j}}{\Delta y} \qquad \text{etc.} \tag{1.41}$$

The discretization process is then repeated in time, to yield a set of algebraic equations (one equation per point and time step). The system is usually coupled.

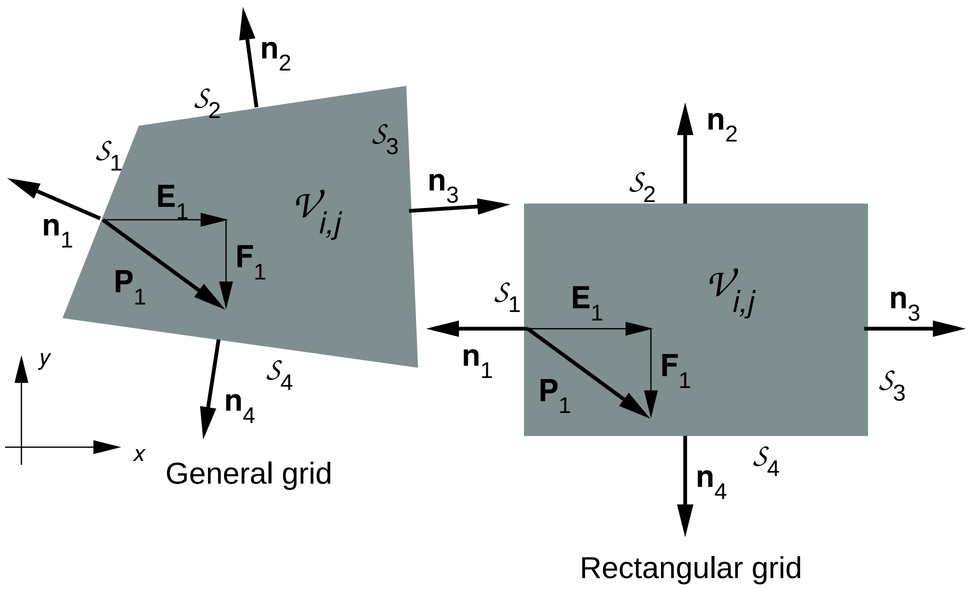

Figure 1.6: Finite-volume approximation in two spatial dimensions.

Finite volumes

In finite-volume methods the discretization generates a number of control volumes. The governing equations are then integrated over the CV, using the variables at the CV centroid to evaluate the fluxes at the faces (*reconstruction*) that appear when the integration is carried out. Finite-differences are used in time, so that an algebraic system (usually coupled) is obtained. Finite-volume schemes are easier to implement than FD on complex non-Cartesian meshes. However, it is hard to obtain high-order approximations.

Example 1:
Integrate the conservation equation

$$\frac{\partial U}{\partial t} + \nabla \cdot \mathbf{P} = Q,$$

where $\mathbf{P} = \mathbf{i}E + \mathbf{j}F + \mathbf{k}G$ (if U were a vector, $\mathbf{P}$ would be a rank two tensor), over the control volume $\mathcal{V}$, assumed fixed in time (so that integration and differentiation commute).

$$\frac{\partial}{\partial t}\int_{\mathcal{V}} U d\mathcal{V} + \int_{\mathcal{V}} \nabla \cdot \mathbf{P} d\mathcal{V} = \int_{\mathcal{V}} Q d\mathcal{V}.$$

Define average values $\overline{f} = \mathcal{V}^{-1}\int_{\mathcal{V}} f d\mathcal{V}$ and apply the divergence theorem to yield

$$\frac{\partial \overline{U}}{\partial t} + \frac{1}{\mathcal{V}}\int_{\mathcal{S}} \mathbf{P} \cdot \mathbf{n} d\mathcal{S} = \overline{Q},$$

where

$$\int_{\mathcal{S}} \mathbf{P} \cdot \mathbf{n} d\mathcal{S} = \sum_{k=1}^{6} \int_{\mathcal{S}_k} \mathbf{P}_k \cdot \mathbf{n}_k d\mathcal{S}_k$$

and the index k indicates the face of the grid cell. The flux on the face, $\mathbf{P}_k$, must be evaluated using the value of $\mathbf{U}$ at the neighboring cells.

Spectral methods

Express the variables as Fourier, Chebychev, Legendre etc. series, use the orthogonality properties of the expansion functions to obtain an ODE per mode (*i.e.*, grid point). Discretize in time to get algebraic equations. Spectral methods are more accurate (for a give grid) than any other method, but are difficult to extend to complex geometries.

1.4.3 Choose the grid

The grid must be able to resolve the important physical phenomena. It can be uniform or stretched, orthogonal or non-orthogonal, structured, block structured or unstructured (See Figs. 1.7 and 1.8).

1.4.4 Choose the order of accuracy

Decide how to evaluate derivatives, integrals, fluxes etc. Higher order ⇒ more accuracy, more expensive (memory, CPU). ⇒ **Discretization errors**.

1.4.5 Choose the solution method

That is, the time-advancement scheme, the solution method for the matrix, the convergence criteria etc. ⇒ **Convergence errors**.

1.5 Example: finite volume method

1.5.1 Choose the model

$$\frac{\partial}{\partial t}\int_{\mathcal{V}} U d\mathcal{V} + \int_{\mathcal{V}} \nabla \cdot \mathbf{P} d\mathcal{V} = 0. \qquad (1.42)$$

Two-dimensional flow.

1.5.2 Choose the discretization method

Finite volumes. Equation (1.42) becomes

$$\frac{\partial \overline{U}}{\partial t} + \frac{1}{\mathcal{V}}\sum_{k=1}^{4} \int_{\mathcal{S}_k} \mathbf{P}_k \cdot \mathbf{n}_k d\mathcal{S}_k = 0 \qquad (1.43)$$

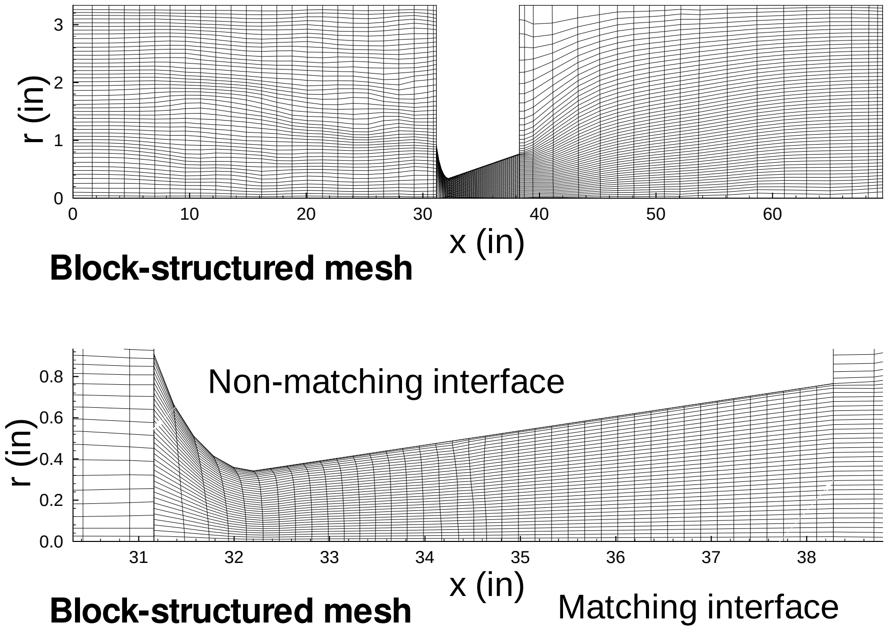

Figure 1.7: Block-structured grid for an axisymmetric pipe-nozzle combination.

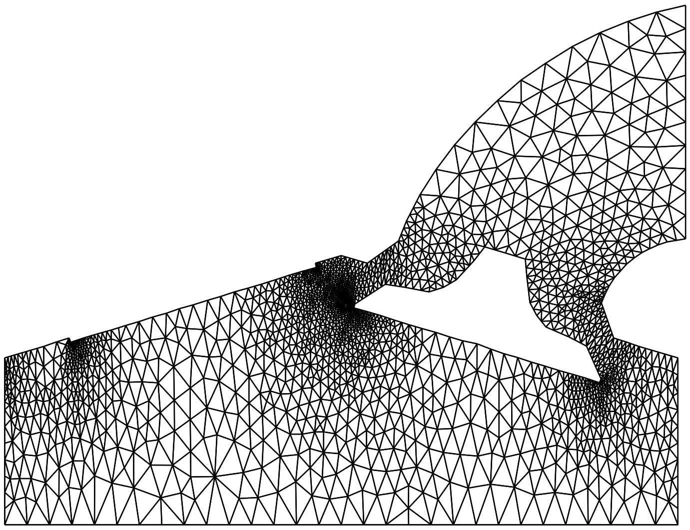

Figure 1.8: Unstructured grid for a cylinder-valve combination.

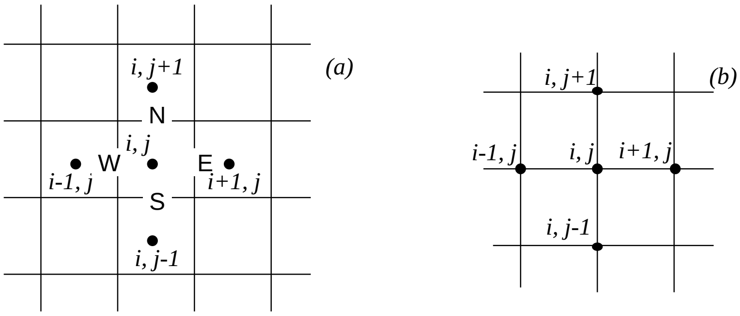

Figure 1.9: Finite-volume (a) and finite-difference (b) grids.

1.5.3 Choose the grid

Uniform cartesian grid, $\Delta x = \Delta y = h$.

1.5.4 Choose the order of accuracy

On the grid in Fig. 1.9, the flux on the E side is

$$\int_{\mathcal{S}_\mathsf{E}} \mathbf{P}_\mathsf{E} \cdot \mathbf{n}_\mathsf{E} d\mathcal{S}_\mathsf{E} = \int_{\mathcal{S}_\mathsf{E}} E_\mathsf{E} dy. \tag{1.44}$$

The order of accuracy is determined by the way this integral is evaluated. For instance, we can assume that E is constant on the E side, and can be extrapolated from its value half-cell to the right (*i.e.*, at point $i+1$). This gives the first-order accurate approximation:

$$\int_{\mathcal{S}_\mathsf{E}} \mathbf{P}_\mathsf{E} \cdot \mathbf{n}_\mathsf{E} d\mathcal{S}_\mathsf{E} \simeq E_{i+1,j} \Delta y. \tag{1.45}$$

Applying the same procedure to the other fluxes gives

$$\frac{d\overline{U}}{dt} + \frac{E_{i+1,j} - E_{i,j}}{\Delta x} + \frac{F_{i,j+1} - F_{i,j}}{\Delta y} = 0 \tag{1.46}$$

1.5.5 Choose the solution method

The time-derivative in (1.46) can be discretized using, for example a backward approximation:

$$\frac{df}{dt} = H \qquad \Rightarrow \qquad \frac{f^n - f^{n-1}}{\Delta t} = H^n \tag{1.47}$$

which gives

$$\frac{\overline{U}^n_{i,j} - \overline{U}^{n-1}}{\Delta t} + \frac{E^n_{i+1,j} - E^n_{i,j}}{\Delta x} + \frac{F^n_{i,j+1} - F^n_{i,j}}{\Delta y} = 0. \tag{1.48}$$

Expressing the fluxes E and F in terms of $\overline{U}$ will give a system of linear/nonlinear coupled/decoupled equations that can be solved by some direct or iterative scheme.

1.6 Example: finite difference method

1.6.1 Choose the model

Again (1.42); two-dimensional flow.

1.6.2 Choose the discretization method

Finite differences.

1.6.3 Choose the grid

Uniform cartesian grid, $\Delta x = \Delta y = h$.

1.6.4 Choose the order of accuracy

On the grid in Fig. 1.9, the spatial derivatives in (1.42) can be obtained by a second-order accurate approximation:

$$\frac{dU_{i,j}}{dt} + \frac{E_{i+1,j} - E_{i-1,j}}{2\Delta x} + \frac{F_{i,j+1} - F_{i,j-1}}{2\Delta y} = 0 \tag{1.49}$$

1.6.5 Choose the solution method

The time-derivative in (1.46) can be discretized using, for example a forward approximation:

$$\frac{df}{dt} = H \qquad \Rightarrow \qquad \frac{f^n - f^{n-1}}{\Delta t} = H^{n-1} \tag{1.50}$$

which gives

$$\frac{U_{i,j}^n - U^{n-1}}{\Delta t} + \frac{E_{i+1,j}^{n-1} - E_{i-1,j}^{n-1}}{2\Delta x} + \frac{F_{i,j+1}^{n-1} - F_{i,j-1}^{n-1}}{2\Delta y} = 0. \tag{1.51}$$

Expressing the fluxes E and F in terms of U will give a system of linear decoupled equations that can be solved by some direct scheme.